



City Research Online

City, University of London Institutional Repository

Citation: MASDARI, M., ZEINALZADEH, A., ABDI, M. A. & SOLTANI, M. R. (2022).
Experimental investigation of shock-buffet criteria on a pitching airfoil. *Chinese Journal of Aeronautics*, 35(7), pp. 179-191. doi: 10.1016/j.cja.2021.08.028

This is the published version of the paper.

This version of the publication may differ from the final published version.

Permanent repository link: <https://openaccess.city.ac.uk/id/eprint/32790/>

Link to published version: <https://doi.org/10.1016/j.cja.2021.08.028>

Copyright: City Research Online aims to make research outputs of City, University of London available to a wider audience. Copyright and Moral Rights remain with the author(s) and/or copyright holders. URLs from City Research Online may be freely distributed and linked to.

Reuse: Copies of full items can be used for personal research or study, educational, or not-for-profit purposes without prior permission or charge. Provided that the authors, title and full bibliographic details are credited, a hyperlink and/or URL is given for the original metadata page and the content is not changed in any way.

City Research Online:

<http://openaccess.city.ac.uk/>

publications@city.ac.uk



Chinese Society of Aeronautics and Astronautics
& Beihang University

Chinese Journal of Aeronautics

cja@buaa.edu.cn
www.sciencedirect.com



Experimental investigation of shock-buffet criteria on a pitching airfoil



Mehran MASDARI^{a,*}, Aghil ZEINALZADEH^b, Mohammad Ali ABDI^b,
Mohammad Reza SOLTANI^{b,c}

^a Faculty of New Sciences and Technologies, University of Tehran, Tehran 1417614418, Iran

^b Department of Aerospace Engineering, Sharif University of Technology, Tehran 11365-11155, Iran

^c Department of Aeronautical and Astronomical Engineering, University of Washington, Seattle, WA, USA

Received 12 January 2021; revised 10 March 2021; accepted 20 April 2021

Available online 28 October 2021

KEYWORDS

Airfoil;
Buffeting;
Experimental analysis;
Hysteresis loops;
Pitching motion;
Shock wave;
Wavelet analysis

Abstract An experimental investigation of the shock-buffet phenomenon subject to unsteady pitching supercritical airfoil around its quarter chord has been conducted in a transonic wind tunnel. The model was equipped with pressure taps connected to the fast response pressure-transducers. Measurements were conducted at different free-stream Mach number from 0.61 to 0.76. The principle goal of this investigation was to experimentally discuss the shock-buffet criterion over a SC(2)-0410 supercritical pitching related to the hysteresis loops of total drag and trailing edge pressure, the behaviour of the shock wave foot location, the pressure distribution over the upper surface, and by implementing the wavelet analysis of the normal force. To ensure capturing the buffet phenomenon by utilizing these criteria, a pressure port has been drilled exactly at the trailing edge of the airfoil where its output was used to detect the buffet phenomenon for different conditions. Visual representation of the flow using the shadow graph flow visualization technique for different test cases is further used to illustrate the unsteady shock wave motion. A comparative analysis of experimental measurements shows that the conducted criteria confirm each other when the buffet phenomenon occurs at the position of the oscillating cycle.

© 2021 Chinese Society of Aeronautics and Astronautics. Production and hosting by Elsevier Ltd. This is an open access article under the CC BY-NC-ND license (<http://creativecommons.org/licenses/by-nc-nd/4.0/>).

1. Introduction

Shock-wave oscillation has been a subject of various studies as early as 1950s.¹ However, after more than sixty years of researches in this exciting field, the Shock-wave/Boundary-Layer Interaction (SBLI) over stationary and oscillating airfoils has not been still fully understood.^{2,3} Transonic buffet occurs when the structure of SBLI bursts⁴ and is often associated with large amplitude, autonomous shock wave oscillations due to the SBLI in which the aerodynamic loads start

* Corresponding author.

E-mail address: m.masdari@ut.ac.ir (M. MASDARI).

Peer review under responsibility of Editorial Committee of CJA.



Production and hosting by Elsevier

to fluctuate at low frequency. Such flow instabilities would limit the flight envelope,⁵ compressor blades,^{6,7} and severe structural vibrations and aileron buzz.^{8,9}

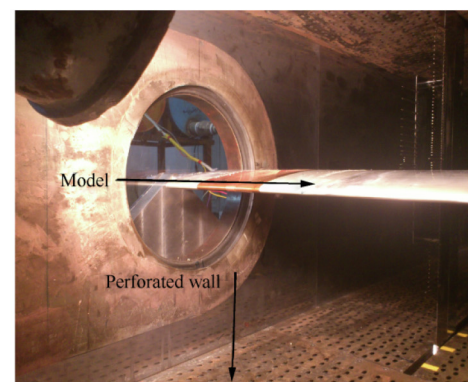
Various criteria have been successfully concluded that are still used as an indication of the buffet onset. Common criteria of the normal force and trailing edge pressure coefficient divergence are investigated by Lee^{4,10}, Polentz¹¹ and Sousa¹² et al. presented a new criterion based on the chordwise movement of the aerodynamic center to estimate the transonic buffet onset of transport aircraft. The application of spectral analysis has also been implemented in numerous researches to extract the characteristic of the shock wave oscillation in a time-frequency domain. Kouchi et al.¹³ experimentally investigated the buffet onset using the wavelet analysis of time-resolved imaging on the upper surface of a fixed mounted supercritical airfoil equipped with vortex generators. A detailed numerical study of the SBLI around a supercritical airfoil at high Reynolds has been conducted by Szubert et al.¹⁴ in which buffet phenomenon was carried out using the Power Spectral Density (PSD) of the wall-pressure fluctuations at three different locations on the surface of the airfoil as well as in the wake. In that work, the amplification of the low-frequency buffet mode in the shock-wave region was also tracked through wavelet analysis. Modal analysis of the shock-buffet is also a powerful mathematical tool to predict the dynamical mode pair or the buffet mode. In this regard, Poplinger et al.¹⁵ and Zhao¹⁶ numerically studied RA16SC1 and OTA15A supercritical airfoils, respectively using the Proper Orthogonal Decomposition (POD) and Dynamic Mode Decomposition (DMD) modal approaches.

Several experimental, as well as numerical kinds of research, have been conducted to describe the buffet mechanism over some of NACA airfoils with and without forced oscillation.¹⁶⁻²² Furthermore, various wind-tunnel tests have been conducted over the matrix of family-related supercritical airfoil developed by NASA, reported by Harris,²³ have been carried out in some significant researches. Zhao et al.²⁴ for instance, investigated the buffet boundaries of a SC(2)-20714 thick supercritical airfoil and utilized RMS of pressure coefficient as a criterion of buffet onset. The principal goal of this contribution is to experimentally gain deep insight of the shock-buffet criterion over a thin airfoil from this family known as SC(2)-0410 under pitching motion. This investigation has been carried out in an open circuit suction-type wind tunnel at various free stream Mach numbers. Preliminary investigations included measurements of the steady pressure distribution and flow visualization at Mach numbers from, $Ma_\infty = 0.27$ to 0.85 for a fixed mounted model. A method to detect the buffet onset based on the surface pressure distribution for that fixed mounted supercritical airfoil was introduced by Golestani et al.²⁵ Moreover, the effects of wall porosity on the flow around this airfoil was investigated.²⁶ Masdari et al.²⁷ experimentally studied the buffet phenomenon over that fixed mounted airfoil at various Mach numbers as well as angles of attack, and found that the buffet onset at $Ma_\infty = 0.66$ and $\alpha = 4.9^\circ$ occurs with frequency of 80 Hz. In addition to the experimental test of this type of supercritical pitching airfoil in transonic regime, further researches about the impact of reduced frequency on the time lag in pressure distribution in a pitch-pause-return motion has been previously investigated.²⁸ Following the experimental studies over SC(2)-0410 supercritical airfoil, in this paper, a detailed discus-

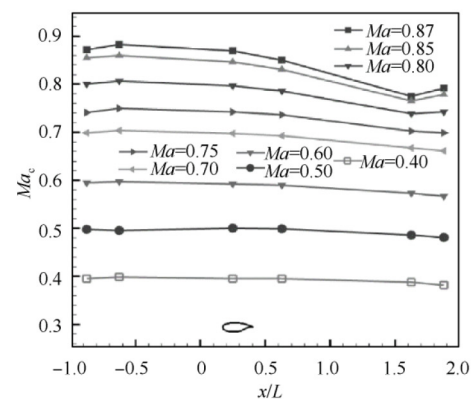
sion of various buffet onset criteria is presented by means of the hysteresis loops of the total drag and trailing edge pressure coefficient, the behaviour of the shock wave foot location, the pressure distribution over the upper surface, and by implementing the wavelet analysis of the normal force integrated from the upper surface pressure distribution of the airfoil.

2. Experimental setup

All experiments were conducted in a transonic wind tunnel. This is a conventional open-return type tunnel with a 60×60 cm² test section and operates at free-stream Mach numbers ranging from $Ma_\infty = 0.4$ to 2.5 thru changing the nozzle profile as well as the engine RPM. The tunnel is equipped with variable perforated walls, ceiling, and floor, to prevent shock reflection during the transonic operations. Fig. 1(a) shows a view of the wind tunnel test section with the perforated walls and a 2D model installed across the side walls. The Mach number distribution along the centerline Ma_c of the test section at transonic speeds for various Mach numbers are shown in Fig. 1(b). The data were obtained by Amiri et al.,²⁹ who studied the steady flow quality assessment of this transonic wind tunnel and improved its performance criterion in the transonic regime based on the operational requirements of the various existing transonic wind tunnels. Vertical lines mark the position of the airfoil in the test section. Apart from this, a chamber was beside the walls to control the



(a) Tunnel test section with a 2D supercritical airfoil model



(b) Mach number distribution along centerline of wind tunnel test section

Fig. 1 Wind tunnel specifications.

boundary layer thickness via an additional power plant system.

All data were collected via an A/D, 24 bit, 64 channels board. Furthermore, data acquisition from high-frequency Kulite sensors (CCQ-093-15D) was done by means of a controller. The nominal and maximum operating pressure was 15 PSI. The maximum reaction time is in order of μs . The maximum error at maximum voltage (100 mV) is 0.1% full scale. The Sampling frequency was set at 2 kHz and a low-pass filter was designed and implemented in the acquisition program with a cut-off frequency of 500 Hz.

All data were acquired at free-stream Mach numbers of $Ma_\infty = 0.27$ to 0.85, but this paper aims to focus on the Mach number ranges between $0.61 < Ma_\infty < 0.76$. The supercritical airfoil oscillated at certain frequencies (f) in pitch at various reduced excitation frequencies (k) as described in Eq. (1), all of which see the Table 1.

$$k = \frac{\pi f C}{U_\infty} \quad (1)$$

According to important researches^{30,31} the resonance and phase lead appeared near the buffet onset when the airfoil forced movement frequency was close to the buffet frequency. The frequency lock-in occurs and stays present until the structural nature frequency is near the double buffet frequency.³² In the present article, the maximum attainable oscillating frequency in the wind tunnel is 9 Hz, corresponding to $k = 0.027$. The maximum natural frequency of the model, including all supports that was calculated, is also about 38 Hz. As discussed in the following sections, the pitching supercritical airfoil would have an extended buffet frequency-band about 80 to 150 Hz, which is too much higher than the maximum oscillating frequency of the pitch motion. Therefore, all results of this paper will not meet lock-in and resonance zones.

The Mach numbers have been determined based upon the previous static tests over this airfoil.²⁷ For the current tests, the pitch motion was of the sinusoidal type motion:

$$\alpha = \bar{\alpha} + \theta \sin(2\pi f t) \quad (2)$$

where $\bar{\alpha}$ is the mean angle attack of the motion, θ is the amplitude.

Attempt to measure pressure distribution of a forced pitching airfoil using Kulite and pressure transducers sensors is a reliable technique in different experimental researches to conduct state-of-the-art measurement techniques. In this regard,

Sugioka et al. installed both Kulite and pressure transducer sensors over the suction side of a NASA Common Research Model (CRM) airfoil and conducted phase-lock lifetime-based Pressure-Sensitive Paint (PSP) technique to obtain pressure distribution on the surface of a pitching airfoil at each phase by the phase-lock method.³³ Fig. 2(a) shows the location of Kulite sensors installed on the upper surface of the present thin SC(2)0410 supercritical airfoil with forced pitching oscillation. The forced oscillations are induced by an electric actuator on one side of the test section, as shown in Fig. 2(b). The airfoil model had a span of 60 cm and a chord (C) of 20 cm.

In addition to the upper surface pressure distribution, two rakes were installed behind the model. The rakes were used to measure the wake profile behind the model, as shown in Fig. 3(a). Due to some limitations, the utmost distance that the rakes could be positioned behind the model was at 30% of the chord, as shown in Fig. 3(b). Since the distance from the airfoil TE to the rake was not far enough to ensure the static pressure recovery within the wake, a static rake was also incorporated in the wake to measure the static pressure inside the wake; hence the wake profile and the corresponding wake drag would be accurate. All pressure ports static and total were connected to very high-frequency Kulite sensors located very close to each port to ensure an accurate unsteady measurement with minimum possible pressure lags. The pressure data's uncertainty was calculated and for all transducers were about 1.8% of their full scale.²⁷

3. Uncertainty

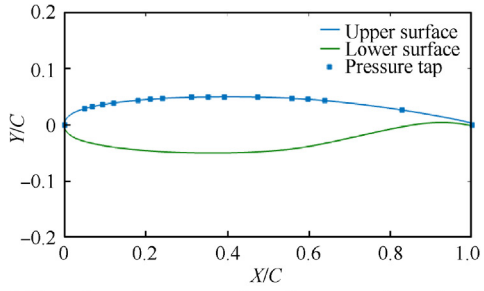
There are two main sources of errors in experimental tests, namely bias and precision. All sensors' bias errors are considered the mean difference between two sets of offset data for a certain pressure transducer sensor. The precision error is also considered as a triple time of the standard deviation for a certain sensor signal. Therefore, one can calculate the uncertainty (U_x) for each sensor from Eq. (3), where B_x and P_x stand for the bias error and precision error, respectively. The total amount of errors of pressure sensors in each test is calculated from Eq. (4).

$$U_x = \sqrt{B_x^2 + P_x^2} \quad (3)$$

$$U_{total} = \sqrt{\sum_{i=0}^n U_{x,i}^2 \left(\frac{\delta y}{\delta x}\right)_i^2}, y = f(x_i) \quad (4)$$

Table 1 Parameters of forced airfoil oscillation, $\frac{x}{C_{rot}} = 0.25$

Case	Ma_∞	$\bar{\alpha}$ (°)	f (Hz)	k	θ (°)
I	0.61	1.1	3	0.009	3.7
II	0.61	1.3	6	0.018	3.9
III	0.61	1.4	9	0.027	1.7
IV	0.61	2.1	5	0.015	6.5
V	0.66	3.3	3	0.008	3.7
VI	0.66	3.2	6	0.017	4
VII	0.71	3.6	3	0.008	3.6
VIII	0.71	3.4	6	0.016	4.1
IX	0.76	1.6	3	0.007	3.8
X	0.76	1.4	6	0.015	4.1

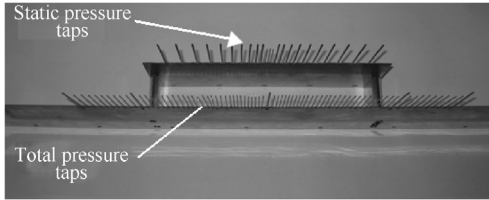


(a) Locations of pressure ports on its upper surface of model

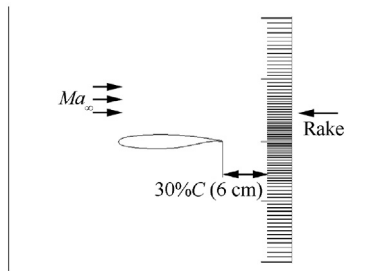


(b) Oscillation mechanism

Fig. 2 Supercritical airfoil model and oscillation mechanism.



(a) Rake system



(b) Position of rake behind model

Fig. 3 Wake measurement mechanism.

Fig. 4 shows the normal distribution of a pressure sensor at $\frac{x}{C} = 0.21$ on the upper surface. The standard deviation of that is also about $\sigma = 1.1040 \times 10^{-5}$. By repeating this procedure for all sensors, it was found that the maximum precision error

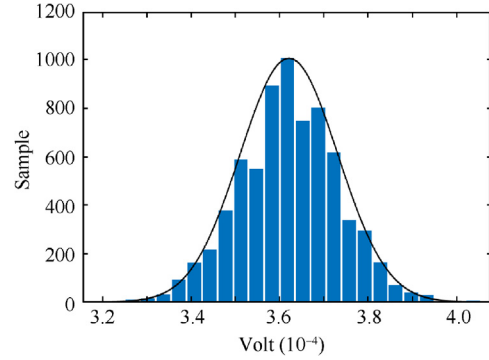


Fig. 4 Normal distribution of a sample sensor at $X/C = 21\%$.

in this experimental investigation was 1.5%. Therefore, the total amount of uncertainty according to Eq. (3) and Eq. (4) will be 1.8%. As proof of successful operation of the same type of sensors at high-speed flow, it should be noted that they were also utilized for inlet buzz measurement, which has a strong connection to the instability of the SBLI.^{34,35}

There are two sources of error for correcting angle of attacks recorded by the accelerometer. The first one arose from the wind tunnel airflow angle indicator, which was reported 0.5 degree by the wind tunnel operators. The second error arose from the oscillator mechanism. According to the results from both the accelerometer and the shadowgraph images calculation, it was found that there was a mean error about 1 degree in all test cases.

One of significant calculation of this study is the estimation of the shock-wave location by means of the pressure distribution of the airfoil and the critical pressure coefficient ($C_{p,c}$) defined by Eq. (5).

$$C_{p,c} = \frac{2}{\gamma Ma_\infty^2} \left[\left(\frac{2 + (\gamma - 1) Ma_\infty^2}{\gamma + 1} \right)^{\frac{\gamma-1}{\gamma}} - 1 \right] \quad (5)$$

In order to calculate the uncertainty of the shock-wave location, the measurement uncertainty of Eq. (5) must be calculated. So, the maximum uncertainty related to the maximum Mach number in the wind tunnel is $U_{Ma_\infty} = 1.3\%$. According to the Eq. (3) and Eq. (4):

$$U_{C_{p,c}} = U_{Ma_\infty} \left(\frac{\delta C_{p,c}}{\delta Ma_\infty} \right) \quad (6)$$

Therefore, at the maximum Mach number $Ma = 0.76$ the total uncertainty related to the $C_{p,c}$ would be about 0.16%.

4. Results and discussion

4.1. Static airfoil results

Fig. 5(a) shows the effects of free-stream Mach number on the wake profile behind the airfoil at various angles of attack. The free-stream Mach number is varied from $Ma_\infty = 0.61$ to $Ma_\infty = 0.76$, and for each Mach number, wake total pressure (P_0) for multiple angles of attack are obtained. The wake profiles obtained from both static and total rakes show that as the angles of attack increase, for a constant Mach number, the wake thickness increases. From this figure, one can calculate

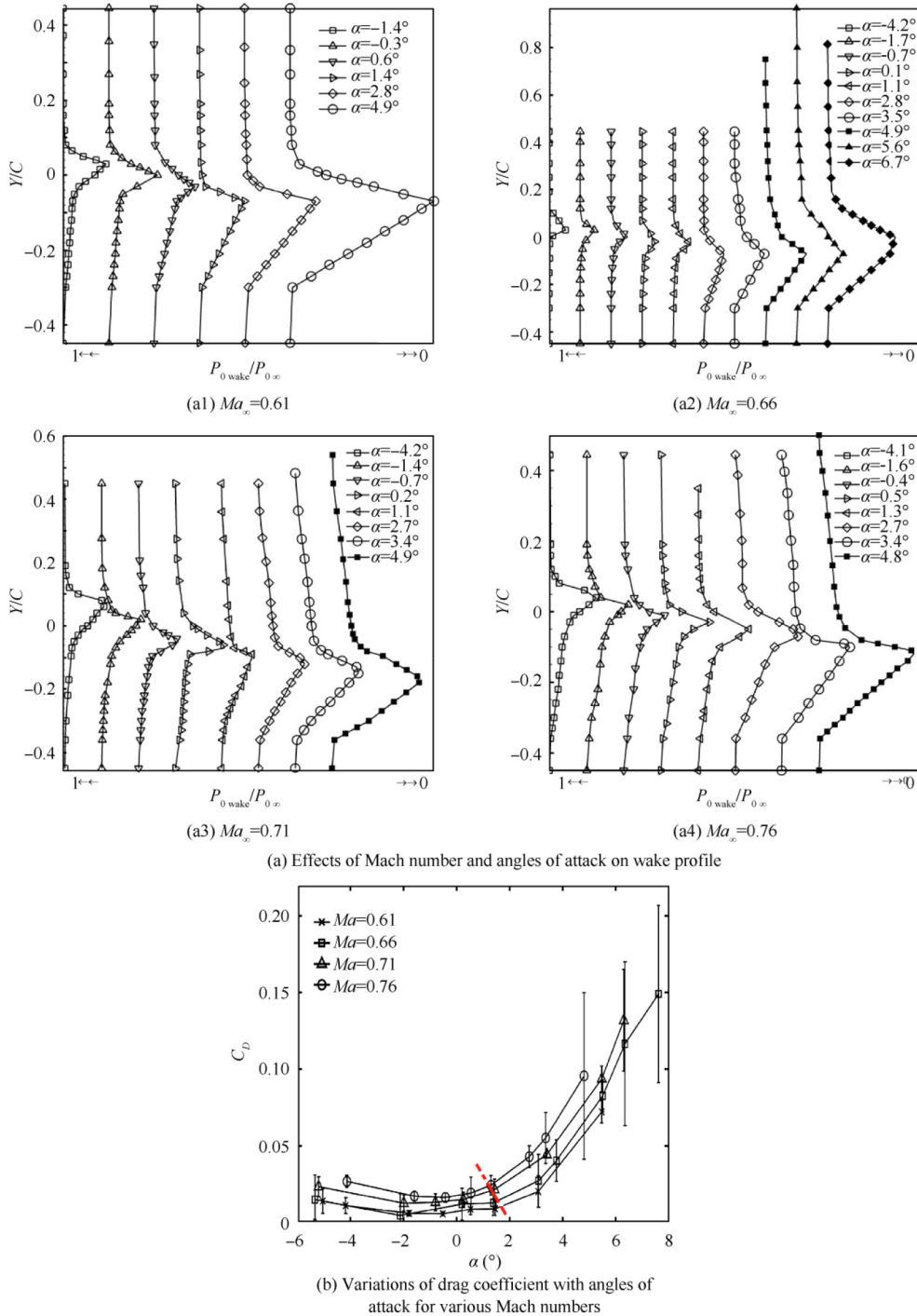


Fig. 5 Effects of angles of attack and free-stream Mach number on wake and drag.

the drag coefficient for each angle of attack for each free stream Mach number. These data are shown in Fig. 5(b). For an airfoil at a certain angle of attack in the flow, as the free-stream Mach number is increased above a particular value, the drag will rise sharply, a phenomenon called drag divergence. Fig. 5(b) shows variations of the drag coefficient (C_D) versus angles of attack (α) for the present supercritical airfoil at several free-stream Mach numbers. The drag divergent for each Mach number can be found in Fig. 5(b). It is taken a point where $\frac{\Delta C_D}{\Delta Ma} \geq 0.05$ and is marked in Fig. 5(b)

as (red line) for each free-stream Mach number. It is clearly seen that the drag divergent point varies with both angles of attack and free-stream Mach number. A hatched line shows that the drag divergence value moves toward the lower angles of attack as the free-stream Mach number is increased from $Ma_\infty = 0.61$ to $Ma_\infty = 0.76$. Furthermore, please note that the precision error bars at high angles of attack are relatively large that may imply massive separation on the airfoil surface and a strong shedding vortex into the wake region.

4.2. Hysteresis loops criterion

The formation of the hysteresis loops at higher Mach numbers is hugely complicated. From the concepts of unsteady aerodynamics, it can be inferred that the load hysteresis loops are formed due to the flow lag and lead phenomenon, such as separation, reattachment, etc., during each oscillating cycle. In an unsteady compressible flow regime around a pitching airfoil, an SBLI may also be formed and then vanish periodically. As soon as the SBLI structure vanishes, the static pressure right at the trailing edge of the airfoil will diverge, and the buffet phenomenon will occur. An advantage of using these hysteresis loops criteria is that they are able to predict how much of a complete cycle is under buffeting flow. Furthermore, when the installation of a pressure port near the trailing edge is not feasible for airfoils having thin trailing edges, hysteresis loops gain an intuitive insight into the phenomenon. Fig. 6 shows variations of $C_{p,te}$, and the wake drag versus the involved hyperparameters. The drag coefficient is obtained by the wake pressure data measured behind the airfoil. The wake pressure was measured by the high-frequency miniature pressure transducers located at the end of the stainless-steel tubes of both total and static rakes to ensure minimum time lag. The measured pressure data for each angle of attack were then integrated to get the corresponding drag coefficient. It is seen that for $Ma_\infty = 0.61$, Fig. 6(a), the trailing edge pressure coefficient loops ($C_{p,te}$) are counterclockwise and do not show severe discrepancies during both upstroke and downstroke motions as well as no sign of divergence is detected from these data. Further, the drag variation loop is clockwise, as seen from Fig. 6-a. In the next case related to $Ma_\infty = 0.66$, Fig. 6(b), there is no fluctuation in the hysteresis loops during the upstroke portion of this motion. However, they cover a significant amount of the cycles when the airfoil in its downstroke phase of the motion, Fig. 6(b). Furthermore, the clockwise hysteresis loops related to $C_{p,te}$ are seen to diverge strongly near the maximum angle of attack. This is a condition where the buffeting phenomenon is believed to occur for the pitching airfoil, which induces a massive flow separation into the wake region periodically and also contributes to the fluctuation of the total drag hysteresis loop, C_D variations in Fig. 6(b). Further, the variation of the drag hysteresis loop changes from a semi-clockwise direction in Fig. 6(a) to the counterclockwise one, Fig. 6(b). The same behaviour is seen for the free-stream Mach number of $Ma_\infty = 0.71$, Fig. 6(c). Fig. 6(d) shows that these fluctuations have covered a larger portion of the cycle, and the directions remain the same as the previous case. According to these results, one can define a criterion for the buffet onset as a condition where the direction of the hysteresis loops of the trailing edge pressure and total drag coefficients with angle of attack turns into clockwise and counterclockwise, respectively, while buffet phenomenon occurs. Interestingly, in this situation, it is seen that the hysteresis loops show fluctuations during a portion of their oscillation cycle.

4.3. Pressure distribution

Fig. 7 shows experimental pressure coefficient C_p distribution on the upper surface of the current airfoil for different conditions. The shock wave location is considered as the intersection

of the pressure distribution with the $C_{p,c}$ line presented in Eq. (5), which the resultant area on the pressure distribution diagram is also known as the supersonic bubble. For $Ma_\infty = 0.61$, (Fig. 7(b)), a small supersonic bubble forms near the leading edge of the airfoil. This bubble is seen to cover a larger portion of the upper surface of the model, and the crest of the pressure distribution is seen to decrease for Fig. 7(c)-(e), which is mostly as a result of increasing the compressibility effects.

To capture the buffet phenomenon, the oscillation cycle is divided into equal phases between $\varphi = \frac{\pi}{2}$ to $\varphi = \frac{3\pi}{2}$, as shown in Fig. 7(a). A sudden variation in the shock-wave foot location during the oscillation occurs. Except for the lowest Mach number, $Ma_\infty = 0.61$, Fig. 7(b), the shock-wave foot location between $\varphi = \frac{\pi}{2}$ and $\varphi = \pi$, moves toward the TE during the oscillation cycle. The maximum mean position of the shock wave foot location reaches about 60% of the airfoil chord at a free-stream Mach number of $Ma_\infty = 0.76$.

Transonic buffet around a pitching airfoil exhibits a complex combination of an unsteady shockwave and boundary-layer phenomena, which is not directly coupled with the shock motion.³ Periodic shock-wave motion over an unsteady airfoil is affected by a change in the state of positioning the effective angles of attack in each phase of the motion. Also, it may oscillate at certain angles of attack due to the buffet phenomenon. In this regard, Tijdeman³⁶ distinguished between three different types of periodic shock-wave motions from the optical flow studies over a NACA64A006 airfoil equipped with an oscillating flap, known as sinusoidal shock-wave motion (Type A), interrupted (Type B), and upstream propagated shock-wave motion (Type C). As a comparison with Tijdeman's work, in the current study, the same types of the oscillating shock wave are seen over the SC(2)-0410 pitching supercritical airfoil. Fig. 8 shows Type B of the shock-wave motion (X_s) versus time period (τ). In this figure, the shock-wave moves almost harmonically, but it disappears during a part of its cosine motion. Because the $C_{p,cr}$ does not intersect with the pressure distribution line. Since the variation in both circulation and apparent mass effects, there exist a significant phase shift between the model cosine motion and the shock-wave location, as clearly seen from Fig. 8. The phase shift increases from $\frac{\Delta t}{\tau} = 0.07$ to $\frac{\Delta t}{\tau} = 0.23$, for Fig. 8(a) and (c), respectively, which is probably due to increasing the reduced frequency from $k = 0.009$ to $k = 0.027$. These small deviations from a pure cosine motion in some test cases are believed to have arisen from the Coriolis force of the rotating mass due to the model movement that leads to small variations of the rotation speed during the oscillating cycle. Such a time lag in the shockwave motion was also previously measured by Hartmann et al.³⁷ about 2.4 ms for a different supercritical airfoil (DRA2303) undergoing different self-sustained coupled heave/pitch motion.

Fig. 9 shows the behaviour of the shock motion in the presence of the buffet. In each case by increasing the angles of attack, the shock-wave moves toward the trailing edge smoothly during the upstroke portion of the oscillating cycle. However, in the downstroke part of the motion the shock-wave encounters strong self-oscillation, which varies with the free-stream Mach number, oscillation frequency, and mean amplitude of the motion. These variations are measured and also change from $\frac{\Delta t}{\tau} = 0.32$ to $\frac{\Delta t}{\tau} = 0.42$. For these cases, the buffet occurs just at the onset of the downstroke portion of the motion.

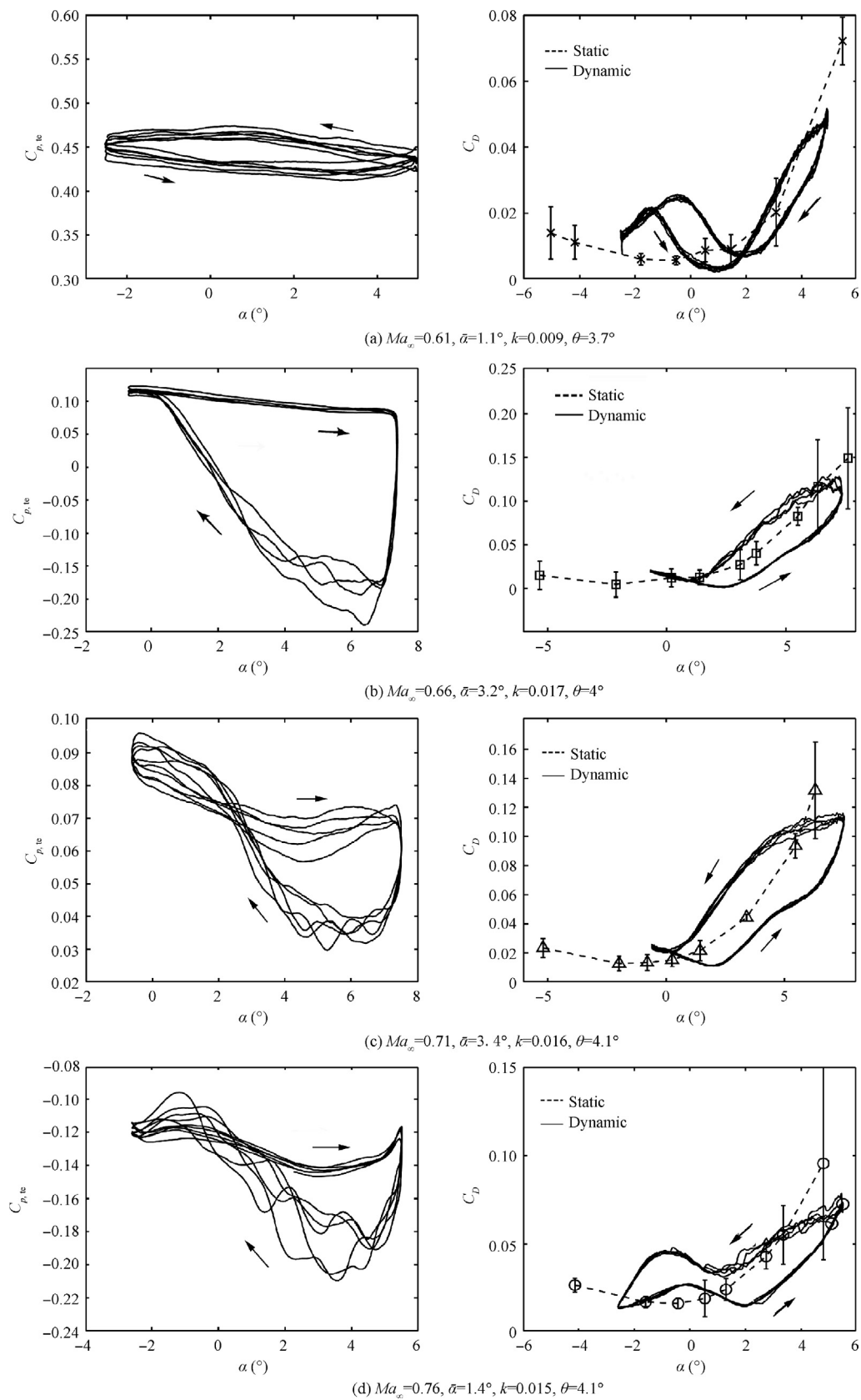
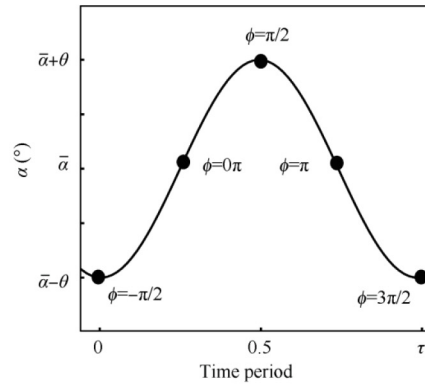


Fig. 6 Total drag hysteresis loops for different test cases.



(a) Schematic of airfoil pitching motion with time

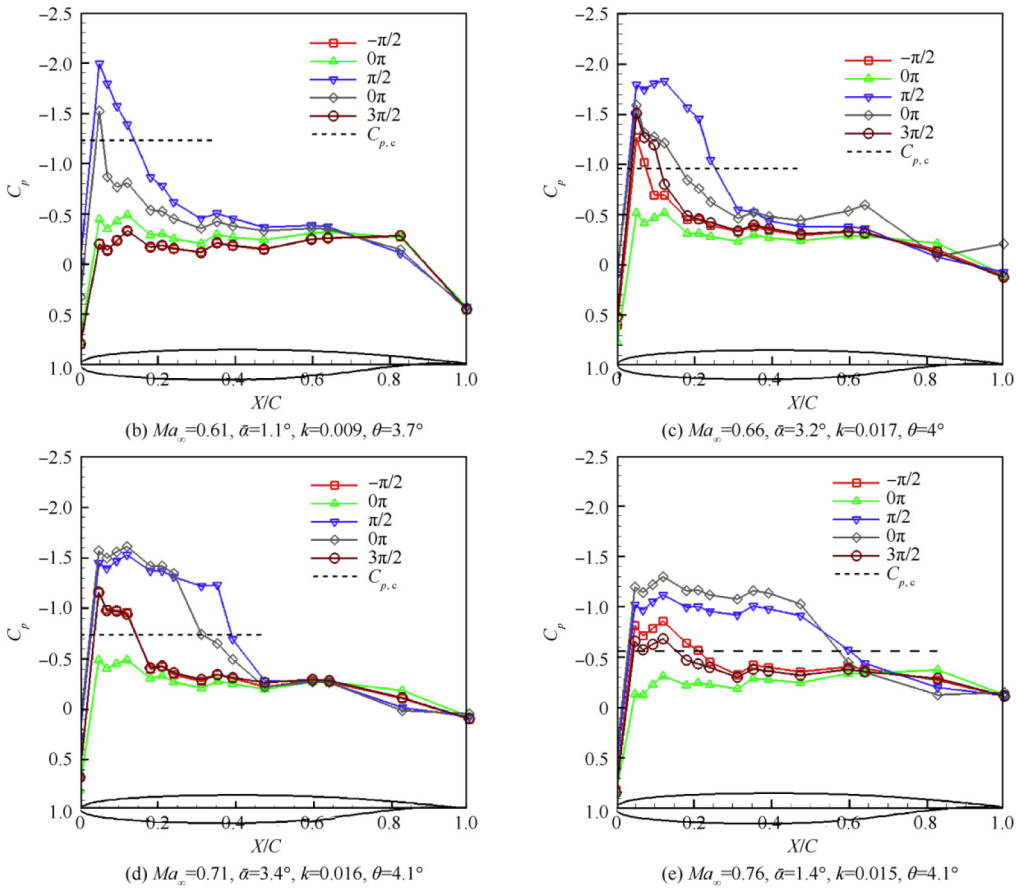


Fig. 7 Pressure distribution over upper surface of airfoil for different test cases.

4.4. Flow visualization

Fig. 10 shows the shadowgraph images for two test cases of $Ma_\infty = 0.61$ and $Ma_\infty = 0.76$ for several segments of the oscillation cycle, $\varphi = -\frac{\pi}{2}$ to $\varphi = \frac{3\pi}{2}$ please refer to Fig. 7(a) for the variations of φ with non-dimensional time. The shadowgraph images show that for the lowest Mach number, $Ma_\infty = 0.61$, a weak shock-wave appears over the surface of the model at $\varphi = \frac{\pi}{2}$ close the leading edge as shown by the letter A. However, for the higher Mach number, $Ma_\infty = 0.76$, a relatively strong moving shock-wave appears over the surface of the model shown by letter C and oscillates back and forth with a certain frequency. In these figures, $\varphi = -\frac{\pi}{2}$ refers to a position

of the airfoil at its minimum angles of attack with no shock-wave forming over the uppers surface. Once the airfoil oscillates with a specified mean angle of attack, both compression and expansion waves are tailored to each other on the surface and form a small supersonic bubble where its location and length vary with the free-stream Mach number, oscillation amplitude, and oscillation frequency, etc. Consequently, a weak shock-wave may form over the surface of the model. When the airfoil is around its mean amplitude, $\varphi = 0\pi$ the compression waves are seen to become stronger and form a relatively strong shock-wave. When the airfoil angle of attack is further increased and reaches close to its maximum amplitude, $\varphi = \frac{\pi}{2}$, a lambda shock-wave forms, as seen from Fig. 10 (b).

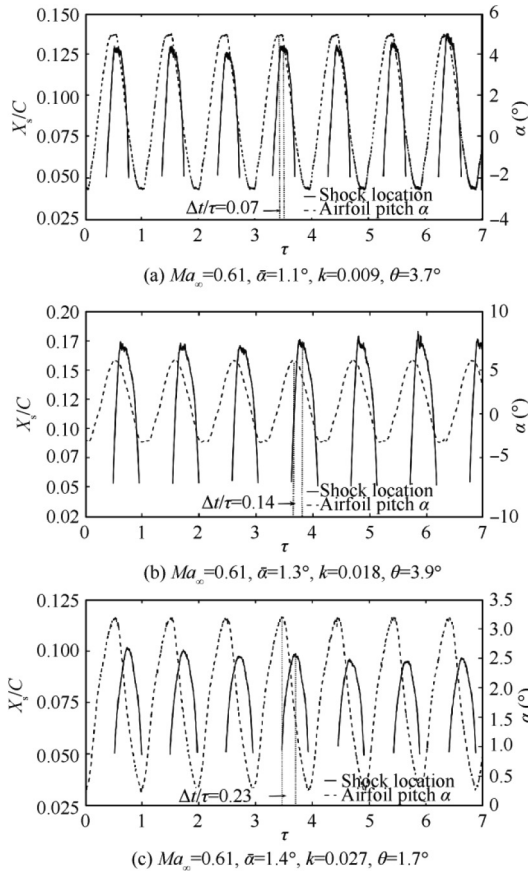


Fig. 8 Effects of oscillating frequency on shock-wave motion (Type B).

This phenomenon stems from the instantaneous acceleration of the flow after the first leg of the shock-wave, terminating with the second leg, consequently the formation of the bifurcated or SBLI structure. When this coalescence of SBLI bursts, it seems that two separated strong oscillating shock-waves appear on the upper surface of the airfoil in the shadowgraph images, as shown by letters C and D in Fig. 10 (b). Since any reaccelerated flow is not seen from the pressure distribution to supersonic flow in Fig. 7 at any phase, it can be claimed that the two appeared shock waves in Fig. 10(b) at $\varphi = \frac{\pi}{2}$ do not physically exist. In fact, there is just single strong shock-wave whose oscillation frequency would be more than the shadowgraph frame rate, 60 Hz.

Once the airfoil angle of attack is reduced to $\varphi = \pi$ and lower, the shock-wave travels toward the leading edge while it encounters self-oscillation. As mentioned before, the amplitude of the shock-wave oscillation reduces and terminates at a certain position on the upper surface during the downstroke portion of the oscillation cycle. By further reduction of the phase motion to $\varphi = \frac{3\pi}{2}$, the shock-waves on the upper surface of the airfoil disappeared.

4.5. Spectral analysis

Fig. 11 shows the power spectral density of the normal force ($C_{N,upper}$) signal for this pitching airfoil for $k = 0.008$ and $k = 0.016$ corresponding to $f = 3$ Hz and $f = 6$ Hz respectively. The dominant lowest frequency seen from these signals

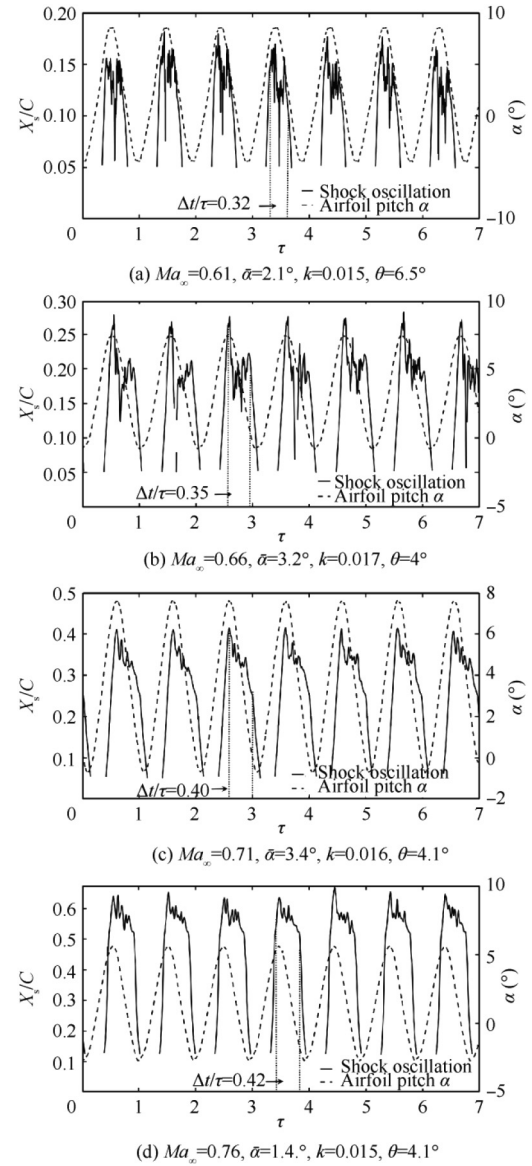
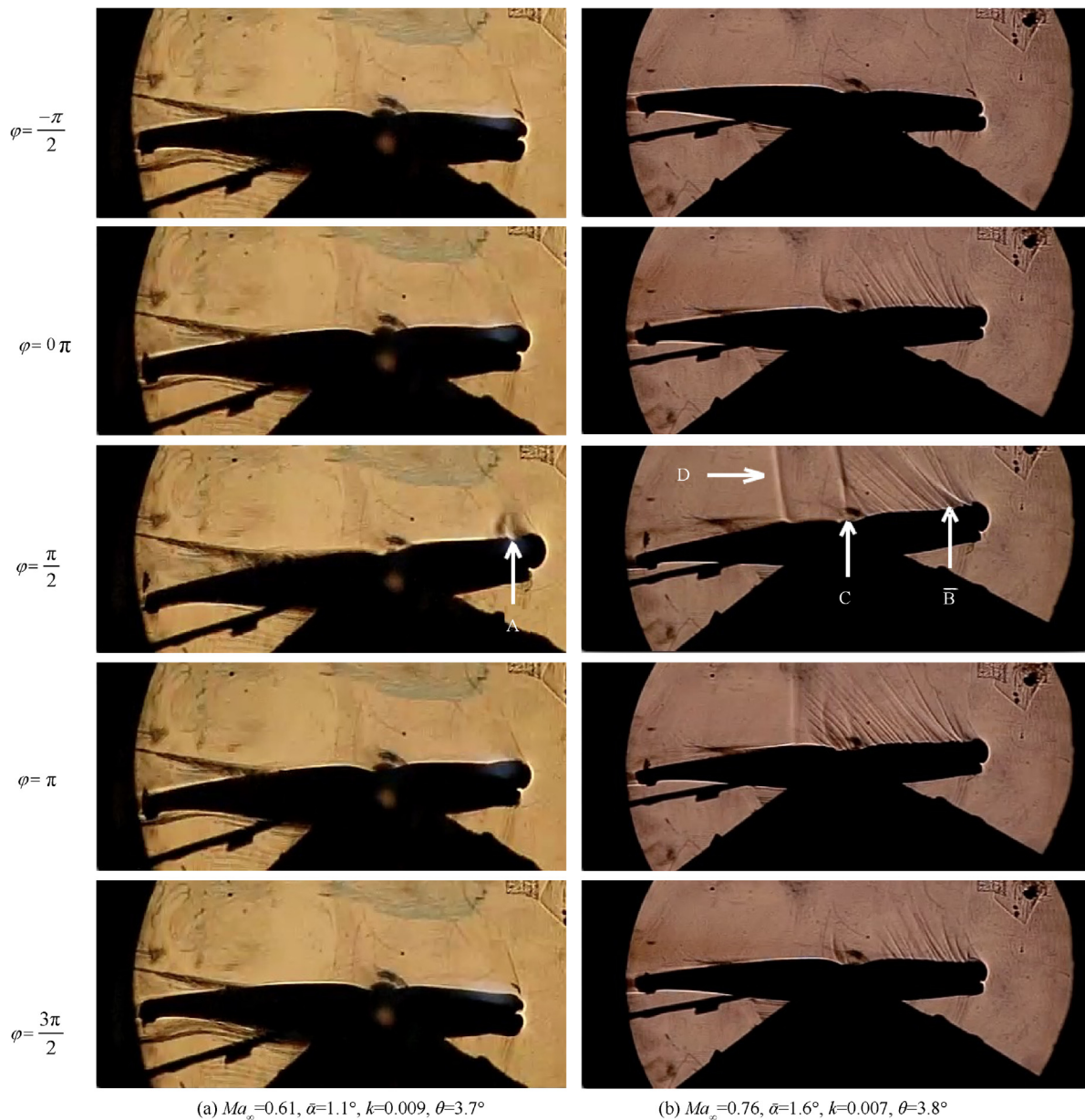


Fig. 9 Shock-wave location at buffet flow for different test cases.

spectral properties stems from the airfoil's periodic motion or the forced oscillation. The other consequent lower spikes are harmonics of the first dominant frequency. Other following narrow band frequency characteristics are considered evidence of the buffet phenomenon for a 2D airfoil model.

The wavelet application will fulfil the lack of spectral information of signal energy in the time domain. For the current tests, all signals recorded by the sensors located on the upper surface of the airfoil experience high transient flow. Therefore, most of the signals are time-domain signals in their raw format and contain dominant spectral components that appear in time. In this paper, the wavelet transforms of the normal force signal calculated by integrating the surface pressure distribution, is obtained. For a good representation of the periodic buffet, the wavelet analysis of the normal force, time history of the motion, as well as the trailing edge pressure coefficient of the airfoil are conveyed into one diagram, named alpha-diagrams; such a figure is shown in Fig. 12 for various cases.



(a) $Ma_\infty=0.61$, $\bar{\alpha}=1.1^\circ$, $k=0.009$, $\theta=3.7^\circ$
 A: Weak shock-wave
 B: Recompression waves
 C: Oscillating normal shock-wave – most forward position
 D: Oscillating normal shock-wave – most aft position

(b) $Ma_\infty=0.76$, $\bar{\alpha}=1.6^\circ$, $k=0.007$, $\theta=3.8^\circ$

Fig. 10 Shadowgraph images for pitching airfoil.

The color ranges for the buffet phenomenon cases are set in such a way that the dominant frequencies above 50 Hz, which are products of energy dissipation, could be presented. The magnitude intervals are much more than the uncertainty of $C_{N,upper}$, as mentioned in the uncertainty section. Nevertheless, in this paper, the spectral properties and qualitative trends are more noticeable. The Morlet function which has a good resolution in the magnitude of the wavelet components is applied. For this analysis, 512 time-scales of the wavelet are used.

As seen from Fig. 12(a), for $Ma_\infty = 0.61$, the lowest Mach number, there are no dominant frequencies at the band of the buffet frequency with high energy level components. The trailing edge pressure coefficient as well as the normal force signals retain near perfect cosine curve without fluctuations. Note the slight fluctuations seen in the $C_{p,te}$ data are believed to be due to the various noises that are unavoidable in experimental studies. As the free-stream Mach number is increased to higher Mach numbers, the wavelet diagram could be divided into at least three different regions, A, B, and C. The bright region

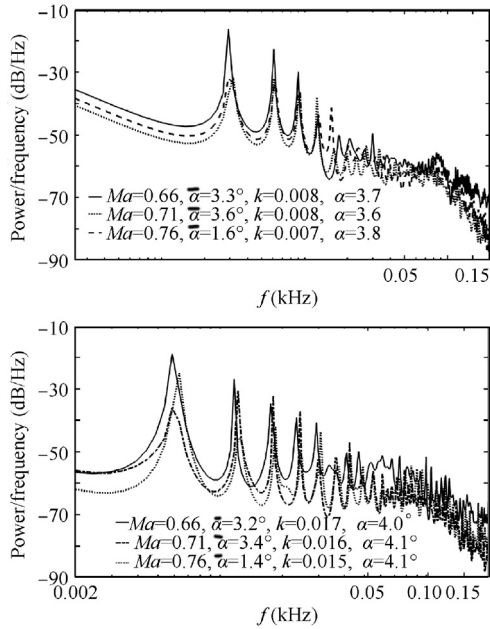


Fig. 11 Power spectrum density of normal force signal for different test cases.

A, as shown in Fig. 12(b), refers to a periodic narrow band of moderate magnitude (energy level) and has a mean frequency of about 20 Hz, which may be created by the coalescence of the recompression waves resulting from the stable shock-wave moving on the upper surface of the airfoil as well as the gradual increment of components of the normal force due to increasing the angle of attack. In this phase of the pitching cycle, the compressibility increases, and a stable shock-wave movement forms without oscillation. From Fig. 12(b) for the ranges of $\varphi = 0$ to $\varphi = \frac{\pi}{2}$ (the variations of $C_{N,upper}$ and α versus τ are shown at the top of Fig. 12(b)) it is seen that by increasing the angles of attack, the normal force becomes too much noisy. Near $\varphi = \frac{\pi}{2}$ the shock-wave intensively starts to oscillate and produces the region shown by the letter B in the figure. This region on the wavelet diagram, which coincides with intense fluctuation of the substantial pressure divergence as well as the normal force diagrams, implies the buffet phenomenon with an extend frequency-band about 80 to 150 Hz. At region C, the mean location of the oscillating-shock-wave moves toward the leading edge, and its strength, as well as its amplitude decrease rapidly. For this situation, the airfoil experiences shock-free flow field, attached boundary layer, and a stable trailing edge pressure coefficient is seen from the variations of $C_{p,te}$ versus τ shown at the top of Fig. 12(b). The same behaviour can be seen in Fig. 12(c), where the compressibility effects increase due to increase of free stream Mach number. The key factor of the wavelet diagrams is that one can declare if the graph colour bar is set in such a way that both strong and small magnitudes, produced by airfoil motion harmonics at low frequencies and by energy dissipation at higher frequencies respectively, could be demonstrated, then the criterion of buffet phenomenon for the pitching airfoil could be the appearance of remarkable wavelet components dissipated toward a higher frequencies

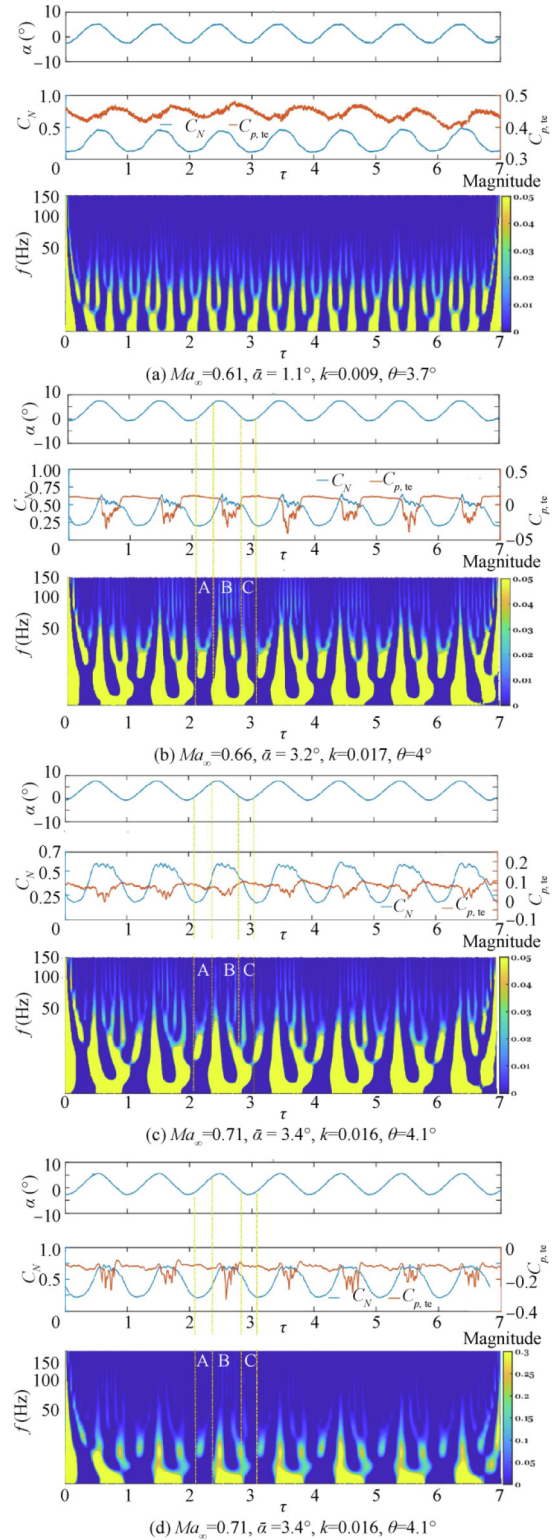


Fig. 12 Wavelet analysis of normal force upper signal for different Mach number.

band in the wavelet diagram of the normal force. In Fig. 12 (d), for instance, the buffet phenomenon cannot be detected due to being set the colour bar at higher value.

5. Conclusions

A forced oscillating SC(2)-0410 supercritical airfoil has been tested under pitching motion in transonic speeds to study the buffet phenomenon via both the pressure distribution over the airfoil and the total drag. The study was carried out by discussing methods of detecting the buffet by means of airfoil hysteresis loops of the total drag and trailing edge pressure coefficient, the behavior of the shock wave location, the pressure distribution over the upper surface, and by implementing the wavelet analysis of the normal force integrated from the upper surface pressure distribution of the airfoil. It was observed that:

- (1) When the airfoil is in its downstroke portion of the cosine motion, the buffet phenomenon occurs, leading to the divergence of the trailing edge pressure. And the normal lift coefficient shows fluctuations during a significant portion of the oscillation cycle. The shadow-graph images also confirmed these observations at the beginning of the downstroke portion of the motion in which the structure of the SBLI bursts and the moving shock-wave begins to fluctuate intensively.
- (2) Once the buffet occurred, the hysteresis loops related to the trailing edge pressure coefficient as well as the total drag coefficient changed their directions to clock-wise and counter-clock-wise, respectively.
- (3) The shock-wave foot location over a pitching airfoil was affected by a change in the effective angles of attack in each phase of the motion. A phase shift between the shock-wave location and the cosine motion of the airfoil was also experimentally measured, which was due to the effects of changes in the circulation and the apparent mass.
- (4) The power spectral of the normal force showed that the dominant frequencies were assigned to the forced-oscillation frequency and its consequent harmonics.
- (5) The wavelet analysis of the normal force signal showed that when the buffet phenomenon occurs, at least three different scenarios in the diagram could be clearly detected, namely the existence of the strong magnitudes, followed by a drastic reduction and dissipation in the magnitude of the dominant frequencies, and lastly an increment in all magnitudes culminating with damping the shock-wave oscillations. Compared with the common criteria for detecting the buffet onset, such as the trailing edge pressure divergence, the wavelet analysis of the normal force is more feasible than constructing an orifice just at the trailing edge of the airfoil, which is difficult and for many thin airfoils is almost impossible.

Declaration of Competing Interest

The authors declare that they have no known competing financial interests or personal relationships that could have appeared to influence the work reported in this paper.

References

1. Humphreys MD. Pressure pulsations on rigid airfoils at transonic speeds. Washington, D.C.: Langley Aeronautical Laboratory, National Advisory Committee for Aeronautics; 195Report No.: RM L51112.
2. Dolling DS. Fifty years of shock-wave/boundary-layer interaction research: what next? *AIAA J* 2001;**39**(8):1517–31.
3. Zauner M, Sandham ND. Modal analysis of a laminar-flow airfoil under buffet conditions at $Re = 500,000$. *Flow, Turbul Combust* 2020;**104**(2-3):509–32.
4. Lee BHK. Self-sustained shock oscillations on airfoils at transonic speeds. *Prog Aerosp Sci* 2001;**37**(2):147–96.
5. Giannelis NF, Levinski O, Vio GA. Influence of Mach number and angle of attack on the two-dimensional transonic buffet phenomenon. *Aerosp Sci Technol* 2018;**78**:89–101.
6. Zeinalzadeh A, Pakatchian MR. Evaluation of novel-objective functions in the design optimization of a transonic rotor by using deep learning. *Eng Appl Comput Fluid Mech* 2021;**15**(1):561–83.
7. Szwaba R, Kaczynski P, Doerffer P. Roughness effect on shock wave boundary layer interaction area in compressor fan blades passage. *Aerosp Sci Technol* 2019;**85**:171–9.
8. Gao C, Zhang W, Ye Z. Reduction of transonic buffet onset for a wing with activated elasticity. *Aerosp Sci Technol* 2018;**77**:670–6.
9. Shinde V, McNamara J, Gaitonde D. Control of transitional shock wave boundary layer interaction using structurally constrained surface morphing. *Aerosp Sci Technol* 2020;**96**:105545.
10. Lee BHK. Effects of trailing-edge flap on buffet characteristics of a supercritical airfoil. *J Aircr* 1992;**29**(1):93–100.
11. Polentz PP, Page WA, Levy LLJ. The unsteady normal-force characteristics of selected NACA profiles at high subsonic Mach numbers. Washington, D.C.: Ames Aeronautical Laboratory, National Advisory Committee for Aeronautics; 1955. Report No.: RM A55C02.
12. Sousa RS, Girardi RD, Annes da Silva RG. A new criterion for transonic buffeting onset estimation. *35th AIAA applied aerodynamics conference*. Reston: AIAA; 2017.
13. Kouchi T, Yamaguchi S, Koike S, et al. Wavelet analysis of transonic buffet on a two-dimensional airfoil with vortex generators. *Exp Fluids* 2016;**57**(11):166.
14. Szubert D, Grossi F, Jimenez Garcia A, Hoarau Y, Hunt JCR, Braza M. Shock-vortex shear-layer interaction in the transonic flow around a supercritical airfoil at high Reynolds number in buffet conditions. *J Fluids Struct* 2015;**55**:276–302.
15. Poplinger L, Raveh DE, Dowell EH. Modal analysis of transonic shock buffet on 2D airfoil. *AIAA J* 2019;**57**(7):2851–66.
16. Zhao Y, Dai Z, Tian Y, Xiong Y. Flow characteristics around airfoils near transonic buffet onset conditions. *Chin J Aeronaut* 2020;**33**(5):1405–20.
17. W.C. Crisler AK. PIV investigation of high speed flow over a pitching airfoil. In *32nd aerospace sciences meeting and exhibit*. Reston: AIAA; 1994.
18. Choudhuri P, Knight D. Effects of compressibility, pitch rate and Reynolds number on unsteady incipient boundary layer separation over a pitching airfoil. *33rd aerospace sciences meeting and exhibit*. Reston: AIAA; 1995.
19. Chen C, Sheu M. Parameter effects on oscillatory aerofoil in transonic flows. *21st fluid dynamics, plasma dynamics and lasers conference*. Reston: AIAA; 1990.
20. Kharati Koopaee M. Effect of flow regime change from subsonic to transonic on the air loads of an oscillating airfoil. *J Fluids Struct* 2014;**50**:312–28.
21. Zhou T, Feng S-S, Dowell EH. Buffeting and lock in of an airfoil at high angle of attack. *J Aircr* 2018;**55**(2):771–80.

22. Zhou T, Dowell E, Feng S-S. Computational investigation of wind tunnel wall effects on buffeting flow and lock-in for an airfoil at high angle of attack. *Aerosp Sci Technol* 2019;**95**:105492. <https://doi.org/10.1016/j.ast.2019.105492>.
23. Harris CD. NASA supercritical airfoils. Washington, D.C.: Langley Research Center, National Aeronautics and Space Administration; 1990. Report No.: TP 2969.
24. Zhao Z, Ren X, Gao C, et al. Experimental study of shock wave oscillation on SC(2)-0714 airfoil. *51st aerospace sciences meeting including the new horizons forum and aerospace exposition*. Reston: AIAA; 2013.
25. Golestani A, Bonab MBE, Soltani MR. An experimental study of buffet detection on supercritical airfoils in transonic regime. *Proc Inst Mech Eng Part G: J Aerosp Eng* 2015;**229**(2):312–22.
26. Golestani A, Soltani MR, Masdari M. Effect of wind tunnel wall porosity on the flow around an oscillating airfoil at transonic speeds. *Sci Iran* 2017;**24**(3):1069–76.
27. Masdari M, Talebi M, Zeinalzadeh A, et al. Experimental investigation of shock wave oscillation on a thin supercritical airfoil. *Sci Iran* 2020;**27**(2):795–805.
28. Eslami HZ, Davari AR, Soltani MR. Impact of reduced frequency on the time lag in pressure distribution over a supercritical airfoil in a pitch-pause-return motion. *Chin J Aeronaut* 2019;**32**(2):243–52.
29. Amiri K, Soltani MR, Haghiri A. Steady flow quality assessment of a modified transonic wind tunnel. *Sci Iran* 2013;**20**(3):500–7.
30. Iovnovich M, Raveh DE. Transonic unsteady aerodynamics in the vicinity of shock-buffet instability. *J Fluids Struct* 2012;**29**:131–42.
31. Raveh DE, Dowell EH. Frequency lock-in phenomenon for oscillating airfoils in buffeting flows. *J Fluids Struct* 2011;**27**(1):89–104.
32. Quan J, Zhang W, Gao C, Ye Z. Characteristic analysis of lock-in for an elastically suspended airfoil in transonic buffet flow. *Chin J Aeronaut* 2016;**29**(1):129–43.
33. Sugioka Y, Nakakita K, Saitoh K, et al. First results of lifetime-based unsteady psp measurement on a pitching airfoil in transonic flow. *2018 AIAA aerospace sciences meeting*. Reston: AIAA; 2018.
34. Daliri A, Farahani M, Sepahi-Younsi J. Novel method for supersonic inlet buzz measurement in wind tunnel. *J Propuls Power* 2018;**34**(1):273–80.
35. Abedi M, Askari R, Soltani MR. Numerical simulation of inlet buzz. *Aerosp Sci Technol* 2020;**97**:105547.
36. Tijdeman H. On the motion of shock waves on an airfoil with oscillating flap. In: Oswatitsch K, Rues D, editors. *Symposium Transsonicum II*. Heidelberg: Springer, Berlin Heidelberg; 1976. p. 49–56.
37. Hartmann A, Klaas M, Schröder W. Coupled airfoil heave/pitch oscillations at buffet flow. *AIAA J* 2013;**51**(7):1542–52.